Case Study

Investigation on the Cause of Damages of a Deep Tunnel

Annamaria Cividini[1]; Alessio Contini[2]; Livio Locatelli[3]; and Giancarlo Gioda, M.ASCE[4]

Abstract: A study is presented on the damages that developed in the segmented precasted concrete liner of a deep tunnel excavated by means of a tunnel boring machine (TBM). Various possible causes are considered i.e., the pore-water pressure acting on the liner; the excessive mountain pressure; the anisotropic in situ stress field; and the incomplete filling of the rock-lining gap. The in situ investigation, carried out to quantitatively assess the level and the extent of the damages, ruled out the pore pressure as the main source. In fact, minor water leakages were observed at the fractured sections. The remaining alternatives were analyzed through a series of nonlinear finite-element calculations in the plane strain regime. They account for the strain softening behavior of the lining and for the lack of tensile stresses at the rock-lining interface. The results give insight into the rock-liner interaction and show that the observed damages are likely to depend on the incomplete filling of the gap. On this basis some conclusions are drawn on the stresses developing within the liner and on the procedures suitable for its structural rehabilitation. **DOI: 10.1061/(ASCE)GM.1943-5622.0000108.**

CE Database subject headings: Damage; Finite element method; Strain; Tunnels; Excavation.

Author keywords: Damages; Finite elements; Precasted lining; Strain softening.

Introduction

The case history discussed here concerns the Sorenberg service tunnel (Falliti and Marchiori 2003) located in the Swiss portion of the Alps mountain chain. The tunnel was excavated using a full face shield tunnel boring machine (TBM). Its permanent lining consists of precasted concrete segments in which the standard steel bars are absent and the reinforcement consists solely of steel fibers. During construction, the gap existing between the liner and rock was filled with selected granular material, referred to as pea gravel (PG).

Starting from the early stages of excavating the lining showed progressive damage represented by fractures located at the tunnel crown and in the vicinity of its springlines, various provisions were adopted to seal them. However, the fractures reappeared and grew after completion of the work. At some locations the fracture widths exceeded 1 cm. The owner was concerned that the progression of the fractures could lead to local failures of the lining and decided to install steel ribs to reinforce the damaged sections. This, on one hand, appeared as the most rapid and effective provision. However, on the other hand, it did not prevent the formation of cracks in other sections of the tunnel and limited the available internal section. The installation of the steel ribs led to two problems: (1) evaluation of the loads acting on the steel ribs to validate their dimensioning and (2) the choice of an alternative method of structural rehabilitation that would stop the damage from extending throughout the tunnel and would not reduce its internal section.

Here, the results are presented of a case study that was undertaken to single out the causes of the observed damage and to provide answers to the aforementioned problems. The study consists of two parts. The first part is based on a detailed survey of the damage and aims to provide a rational criterion for the installation of steel ribs in previously damaged sections and at sections where fractures develop over time. The second part intends to single out the actual causes of the damage among various possible hypotheses, namely: the excessive mountain pressure with respect to the concrete strength; the anisotropic in situ stress field; the water pressure on the lining; and the incomplete PG filling of the gap between the liner and surrounding rock.

A plane strain finite-element (FE) model was developed for this purpose, where the rock was elastic perfectly plastic while the fiber-reinforced concrete had a strain softening behavior. A Mohr-Coulomb yield condition with a tension cutoff and a nonassociated flow rule was adopted for both materials. The closure of the possible empty gap was accounted for by modifying the mesh geometry during the step-by-step calculations and by allowing for the onset of local contacts between the rock and liner.

The aforementioned assumptions deserve some comments. The plane strain regime seems reasonable because the damage showed up at an appreciable distance from the excavation head and, hence, should not be influenced by the three-dimensional effects developing at the face. In addition, most of the damage involved a number of adjacent rings. These facts suggested that the plane strain assumption should provide a reasonable approximation of the actual field behavior.

In the present context the onset of fractures is mainly governed by the attainment of excessive tensile stresses in the liner. This led to the use of the Mohr-Coulomb yield condition with a tension cutoff and of an elastic-plastic law allowing for the strain softening behavior. The possible variation of the friction angle with increasing (compressive) volumetric stresses was neglected because its effects seemed marginal for the overall behavior of the opening.

In the following, the tunnel characteristics and the results of the in situ survey are presented first. On their bases an empirical criterion is proposed for the installation of steel ribs in those sections where the damage developed over time. Then, the available mechanical

[1]Dept. of Structural Engineering, Politecnico di Milano, Piazza Leonardo da Vinci 32, 20133 Milano, Italy (corresponding author). E-mail: annamaria.cividini@polimi.it

[2]Golder Associates S.R.L., via Decembrio 28, 20137 Milano, Italy. E-mail: alessio.contini@gmail.com

[3]Golder Associates S.R.L., via Decembrio 28, 20137 Milano, Italy. E-mail: livio.locatelli@gmail.com

[4]Dept. of Structural Engineering, Politecnico di Milano, Piazza Leonardo da Vinci 32, 20133 Milano, Italy. E-mail: giancarlo.gioda@polimi.it

Note. This manuscript was submitted on June 13, 2010; approved on December 27, 2010; published online on November 15, 2012. Discussion period open until May 1, 2013; separate discussions must be submitted for individual papers. This paper is part of the ***International Journal of Geomechanics***, Vol. 12, No. 6, December 1, 2012. ©ASCE, ISSN 1532-3641/2012/6-722–731/$25.00.

Int. J. Geomech. 2012.12:722-731.

information for the rock mass (RM), concrete and PG and the results of the FE analyses are illustrated. These results ruled out water and the mountain pressures and the anisotropic in situ stresses as possible causes of the damage and showed that the fractures were likely a result of the incomplete filling of the rock-liner gap. Based on the numerical results, the characteristics of the steel ribs necessary to stabilize the opening are assessed. Some comments are also presented on alternative methods for structural restoration that should avoid the extension of damage to further liner rings over time.

Tunnel Characteristics and Observed Damage

The Sorenberg tunnel is located in the Swiss part of the Alps mountain chain, has a length close to 5 km, an internal diameter of about 4 m, and a cover depth reaching 550 m. The tunnel, excavated using a full face shield TBM, crosses various rock formations of flysch, marl, shale, and limestone (see Fig. 1); its cross section is shown in Fig. 2. Its liner consists of circular rings having a length of 1.5 m in the direction of the tunnel axis. Each circular ring is formed by six precasted concrete segments reinforced solely through steel fibers and connected by waterstop joints. The segments have a thickness of 25 cm and their external radius is 2.15 m, while the radius of the excavation is 2.3 m. Consequently, a gap exists between the rock and liner having a nominal thickness of 15 cm. The rings are placed on a layer of lean concrete that fills the lower part of the rock-liner gap. The upper part of the gap has an extension of 120−130° on both right and left sides from the tunnel crown and, after installation of the segments, was filled with PG.

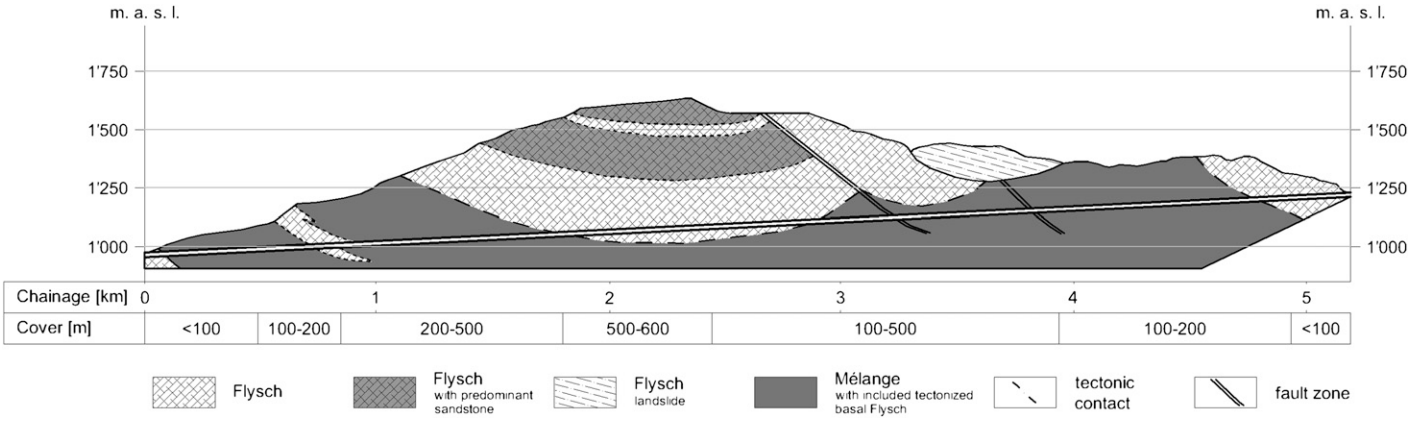

Fig. 1. Longitudinal section of the tunnel

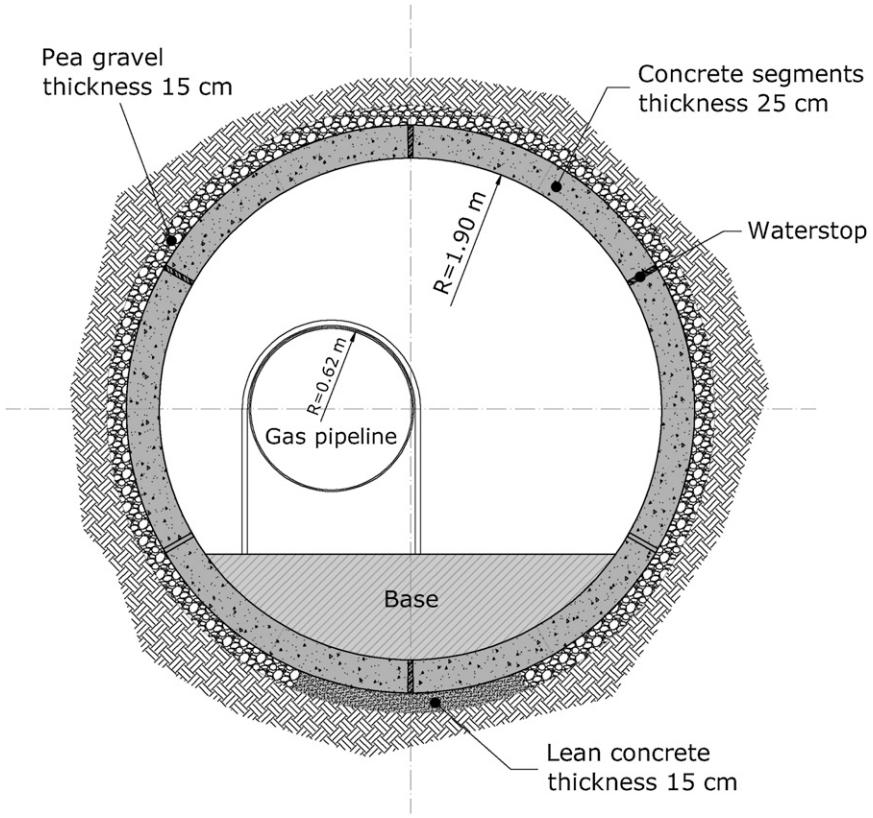

Fig. 2. Tunnel cross section

Int. J. Geomech. 2012.12:722-731.

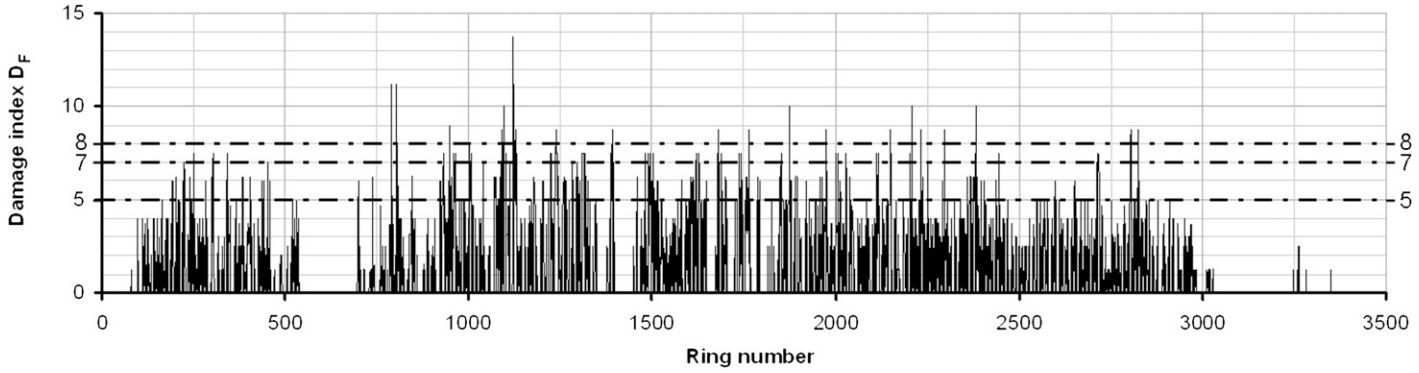

Fig. 3. Distribution of the damage index D_F along the tunnel

At the beginning of this study, several rings were already fractured and were supported by steel ribs. A survey was then undertaken to quantitatively assess the extension of the damaged portions of the tunnel and to formulate a criterion for reinforcing the rings, in particular those where new cracks developed over time. It turned out that about 37% of the rings were damaged. During the survey only minor water leakage was observed at a few fractured sections. This indicated that the water pressure on the tunnel lining was negligible and that it could not be the main cause of the damage.

An attempt to establish a statistical correlation between the location of the fractured rings, the severity of their fracturing, the rock type and the depth of the cover did not lead to consistent results. Consequently, an empirical damage index D_F was defined to evaluate the state of each ring and to allow for a rational choice of the sections where the steel ribs must be installed

$$D_F = \alpha_F \cdot (D_C + D_{RS} + D_{LS}) \quad (1)$$

where indices D_C, D_{RS}, and D_{LS} = crown, right shoulder, and left shoulder of the ring, respectively, depend on the state of fracturing observed. These indices vanish if no fractures are present in the corresponding portion of the ring, while they range from 1 to 4 in the case of damage.

The value of 1 is assigned to an index when a very limited amount of damage is observed; e.g., in the case of a single closed crack with a length that does not reach the length of the ring in the direction of the tunnel axis. A value of 4 denotes one or more open cracks, with appreciable thickness throughout the entire length of the ring. Values of 2 and 3 are assigned to indices D_C, D_{RS}, and D_{LS} in the intermediate conditions.

The coefficient α_F was introduced for two reasons. First, it accounts for the fact that a sequence of two or more fractured rings is potentially more dangerous than an isolated one. In addition, this coefficient increases the value of D_F when only one segment of the ring is damaged. In fact, this condition indicates the initiation of fracturing and should not be overlooked when deciding on the installation of additional steel ribs. The following three values of α_F were adopted: $\alpha_F = 1.25$ when the examined ring belongs to a sequence of adjacent fractured rings or when only one of its concrete segments is damaged; $\alpha_F = 2.5$ if both conditions occur; otherwise, $\alpha_F = 1$.

Applying the described criterion, a maximum value of 13 was obtained for damage index D_F. Figs. 3 and 4 show the distribution of D_F along the tunnel and the diagram of the cumulated number of damaged rings versus D_F, respectively. Based on this, the following suggestions were formulated:

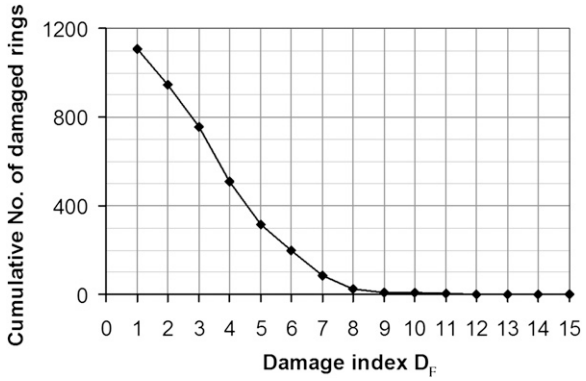

Fig. 4. Cumulated number of the fractured rings versus damage index D_F

- As a first and rapid rehabilitation measure, install steel ribs at rings having $D_F \geq 8$;
- Evaluate the need of installing steel ribs when $8 \geq D_F \geq 7$;
- Monitor the increase of the crack width over time for rings having $7 \geq D_F \geq 5$; and
- Systematically survey the entire tunnel to detect the formation of cracks in previously undamaged rings.

At this stage of the study the problem of determining the characteristics of the steel ribs necessary to stabilize the damaged sections arose. This, in turn, required identification of the causes of fracturing and the estimation of the rock pressure acting on the lining and the ribs. The experimental and numerical study carried out to address this issue is summarized in the subsequent sections.

Material Characterization

An experimental investigation was carried out to complete the available information on the mechanical properties of the relevant materials. It included the determination of the rock-quality designation (RQD) from the borings; in situ pressuremeter tests and laboratory tests on recovered samples of rock, fiber-reinforced concrete, and PG.

The numerical analyses that will be subsequently discussed concern a severely damaged section with a depth of cover of 450 m. The following parameters characterize the rock at that location:

- RQD (ranging between 10 and 50%);
- RM elastic modulus from Menard pressuremeter tests (E_{RM} = 1.2 GPa);

Int. J. Geomech. 2012.12:722-731.

- Intact rock elastic modulus from unconfined compression tests ($E_{laboratory}$ = 54 GPa);
- Intact rock unconfined compression strength ($\sigma_{laboratory}$ = 110 MPa); and
- Residual friction angle from direct shear tests under constant vertical load (φ_{res} = 27°).

The conservative assumption was introduced in the calculations that the friction angle of φ_{RM} coincides with φ_{res}.

The plastic potential is based on the same equation expressing the Mohr-Coulomb criterion but neglecting the cohesive contribution. Lacking the triaxial test results, the angle of plastic dilation ψ_{RM} was derived from the change in thickness of the samples subjected to shear tests. This led to a moderate value of ψ_{RM}, of the order of 5−6°.

While the intact rock cohesion, $c_{laboratory}$, can be easily evaluated knowing the laboratory unconfined compression strength, $\sigma_{laboratory}$, and the friction angle, φ_{res}, the estimation of the in situ cohesion, c_{RM}, is a controversial problem. For instance, it could be assumed that the fractures and joints present in the RM have the same influence on both the elastic modulus and cohesion. In this case, the ratio between laboratory $E_{laboratory}$ and in situ E_{RM} elastic moduli would coincide with that between laboratory $c_{laboratory}$ and in situ c_{RM} cohesion. Under this assumption c_{RM} = 750 kPa is obtained. However, considering the low RQD that characterizes part of the recovered rock, the in situ cohesion could be lower than the one previously evaluated. For this reason some of the calculations were repeated with c_{RM} = 200 kPa, which is considered a particularly conservative value for this parameter.

Several samples of PG were subjected to confined compression tests, using a large size oedometer, and to multistage triaxial tests. It may be observed that the PG is quite uniform throughout the tunnel because its grain size distribution was carefully controlled before filling the rock-liner gap. This led to a marginal variation of the experimental data obtained for the various tested samples. The first group of tests provided the elastic modulus of PG in confined conditions, similar to those present within the rock-liner gap, while the second group led to its friction angle. The corresponding experimental diagrams are shown in Figs. 5 and 6.

The tangent modulus for moderately dense material is about 50 MPa and increases up to 120 MPa after some loading/unloading cycles. The friction angle is close to 40°. The limited compaction to which the PG was subjected during its injection suggested using an elastic modulus E_{PG} = 50 MPa in the calculations. Considering that the thin layer of PG represents an interface between the rock and liner, and that the friction angle of the rock (φ_{RM} = 27°) is lower than that of the PG (40°), in the calculation a friction angle of φ_{PG} = 27° was also adopted for the interface.

For the fiber-reinforced concrete, the unconfined compression tests led to an elastic modulus E_C of about 47 GPa and to a compression strength σ_C between 73 and 119 MPa. Also, tensile tests were carried out on this material (see Fig. 7). Before subjecting the samples to increasing elongation, a thin circumferential indent was produced at the midheight to allow for the propagation of a crack. These tests, which provided a tensile resistance of 4.6 MPa, were numerically simulated in axisymmetric conditions discretizing one-fourth of the sample into the grid of 4-node isoparametric elements shown in Fig. 8. An elastic-plastic strain softening behavior was adopted in the calculations (Cividini and Gioda 1992) obeying the Mohr-Coulomb yield criterion. The friction angle was constant during the analysis, while the cohesion decreased according to the scheme depicted in Fig. 9. The peak cohesion c_P was adopted during the step-by-step calculation until a first limit value γ_P^* of the square root of the second invariant of the deviatoric plastic strains was attained. Then, the cohesion linearly decreased with the plastic strains and reached its residual or ultimate value c_r when a second limit deformation γ_r^* was attained.

The four material parameters, c_P, c_r, γ_P^*, and γ_r^* were calibrated to reach a reasonable agreement between the experimental (Fig. 7) and numerical (Fig. 10) results. The numerically evaluated tensile and compressive strengths were, respectively, 4.4 and 85 MPa, which seemed an acceptable approximation of the corresponding experimental data; i.e., a tensile resistance of 4.6 MPa and uniaxial compression strength between 73 and 119 MPa.

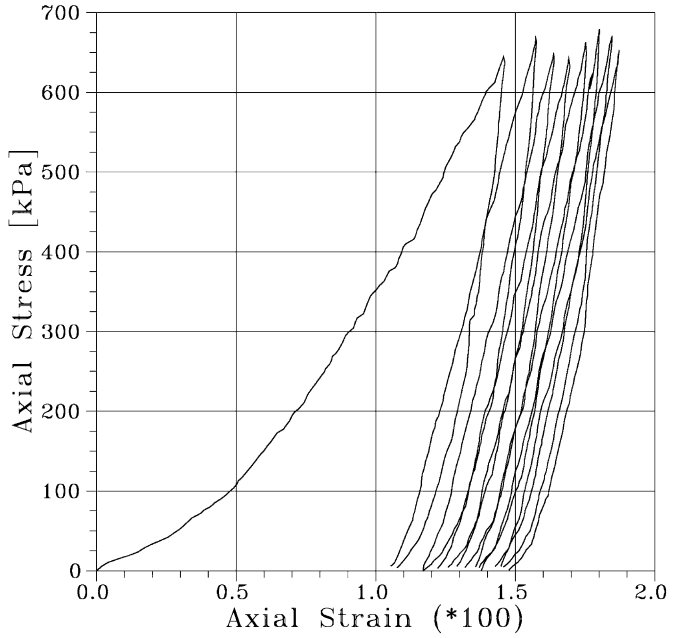

Fig. 5. Results of confined compression test on PG samples

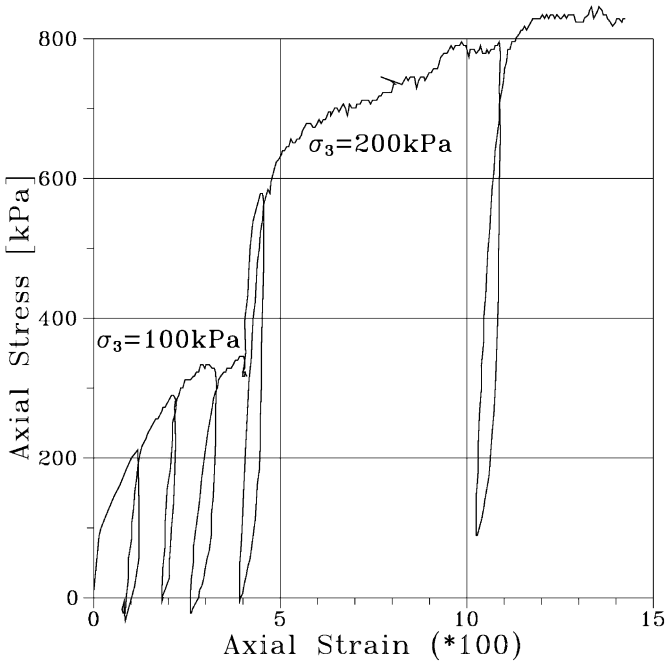

Fig. 6. Results of triaxial test on PG samples

Int. J. Geomech. 2012.12:722-731.

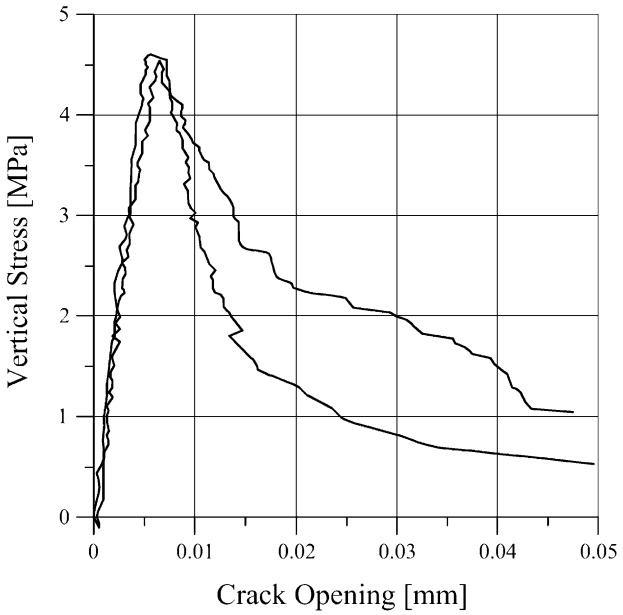

Fig. 7. Experimental results of two tensile tests on concrete samples

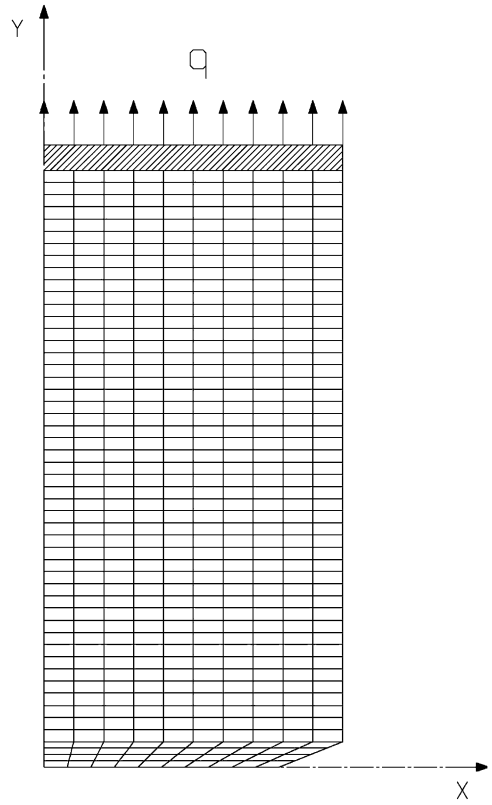

Fig. 8. FE mesh for the numerical simulation of the tensile tests on concrete samples

The mechanical parameters adopted in the calculations are summarized in Table 1 for convenience. A tension cutoff was also introduced for the cohesive materials corresponding to one-tenth of their unconfined compression strengths. However, this had little influence on the numerical results because the tensile behavior of concrete is governed by the aforementioned strain softening law.

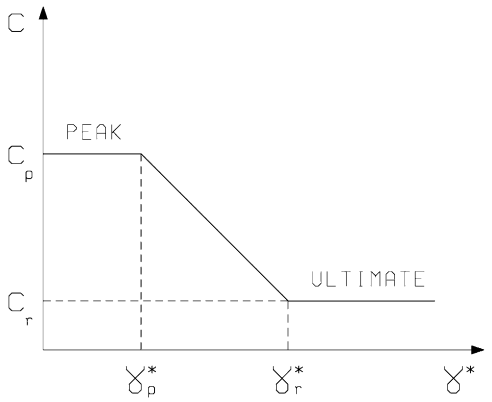

Fig. 9. Scheme of the adopted strain softening behavior

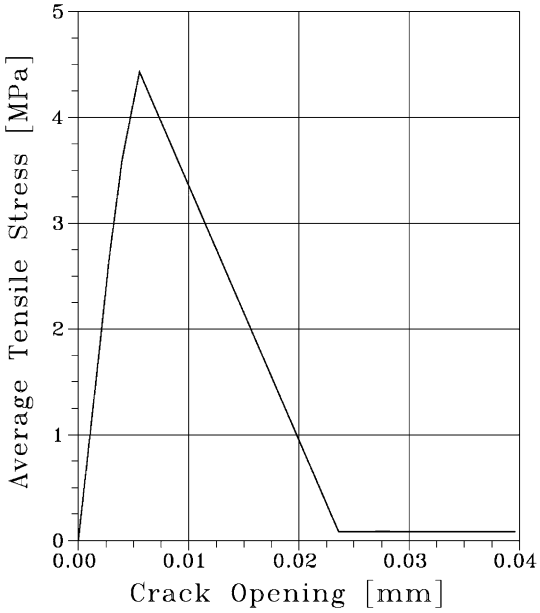

Fig. 10. Numerical simulation of tensile tests on concrete samples

Table 1. Values of the Material Parameters Adopted in the Numerical Analyses

Material	E (MPa)	υ	ϕ (°)	c (kPa)	ψ (°)
RM	1,200	0.25	27	200–750 (range)	6
Concrete	47,000	0.16	40	20,000 (peak); 0 (residual)	8
PG	50	0.25	27	0	6

Note: E = elastic modulus; υ = Poisson ratio; ϕ = friction angle; c = cohesion; ψ = plastic dilation angle.

Numerical Study

The numerical analyses of the rock-liner interaction were based on the noncommercial Code SoSIA-2 for soil/structure interaction analysis (see, for example, Cividini and Gioda 1992; Contini et al. 2007; Sterpi and Gioda 2009). The calculations were carried out assuming (1) the plane strain regime and (2) symmetric conditions about the vertical axis through the tunnel centerline.

The adopted FE grid, a detail of which is shown in Fig. 11, consisted of 2,970 nodes and of 2,680 quadrilateral, 4-node isoparametric elements that discretized the rock, liner, and PG. The

Int. J. Geomech. 2012.12:722-731.

steel ribs were modeled thorough 134 linear beam elements. The shear interaction between the liner and steel ribs was neglected in the calculations considering its limited effect on the overall behavior of the opening.

As previously mentioned, one of the investigated causes of damage is the possible partial filling of the rock-liner interface. Considering that this empty gap is likely to be present in the vicinity of the tunnel crown, where fractures are observed, the upper part of the mesh was refined to improve the accuracy in evaluating the spread of the damage within the top portion of the lining. The angle α denotes the extension of the empty gap in Fig. 11. Lacking any information on the possible geometry of the unfilled gap, its symmetry was assumed with respect to the tunnel centerline. This seems to be a conservative assumption because it may lead to the evaluation of particularly severe stresses in the liner.

A first set of analyses was carried out to estimate the stress state in the liner assuming a complete filling of the gap i.e., $\alpha = 0°$. The results are shown by the diagrams in Figs. 12 and 13 for various values of the coefficients of the rock pressure at rest, K_0, namely, 1.0 and 0.5. In these diagrams P_0 represents the geostatic vertical pressure and P is the decreasing pressure on the opening contour. The calculations were based on the assumption that the liner and the PG filling are set in place when the radial displacements of the opening contour correspond to a pressure P equal to 20% of in situ stresses P_0. In fact, this seems to be a conservative assumption according to the observations contained in AFTES (1993). In addition, this led to normal stresses in the liner that were consistent with the stresses evaluated in the design where the complete filling of the rock-liner interface was implicitly assumed.

Because of uncertainties in evaluating the overall cohesion c_{RM} of the RM, the calculations were repeated by adopting two values for this parameter; namely, 750 and 200 kPa. Only the results of the latter case are shown in Figs. 12 and 13 and correspond to the maximum compressive stresses in the liner of the order of 20−30 MPa, far below the limit resistance of concrete, while no tensile stresses were evaluated. The small difference between the vertical and horizontal convergences for $K_0 = 1$ is a result of the different size of the elements adopted for the upper and lower parts of the mesh.

These results rule out the genuine mountain pressure and the anisotropic in situ stresses as possible causes of the observed damage. As previously observed, because the pore-water pressure on the liner was likely to be moderate, the only remaining cause of damage was the incomplete filling of the rock-liner gap. The consequent elastic-plastic analyses were carried out by decreasing pressure P in small increments and updating the nodal coordinates at the end of

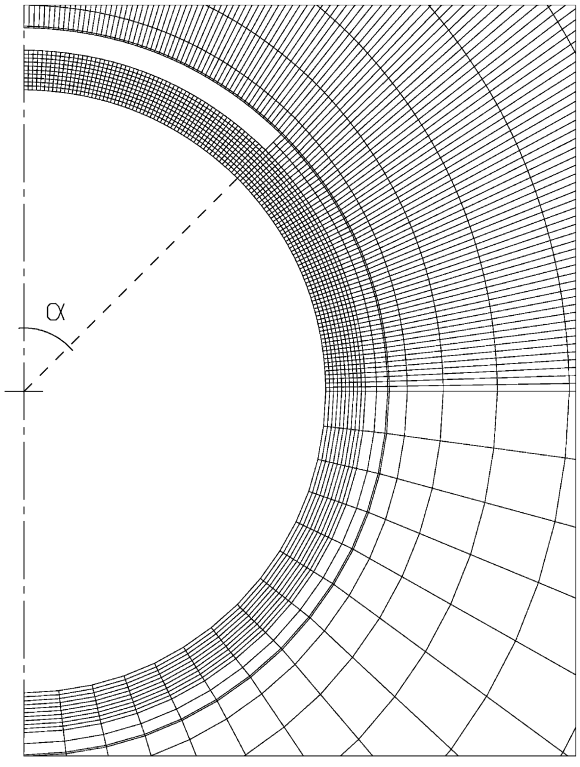

Fig. 11. Detail of the FE mesh in the vicinity of the tunnel (angle α defines the portion of the unfilled rock-liner gap)

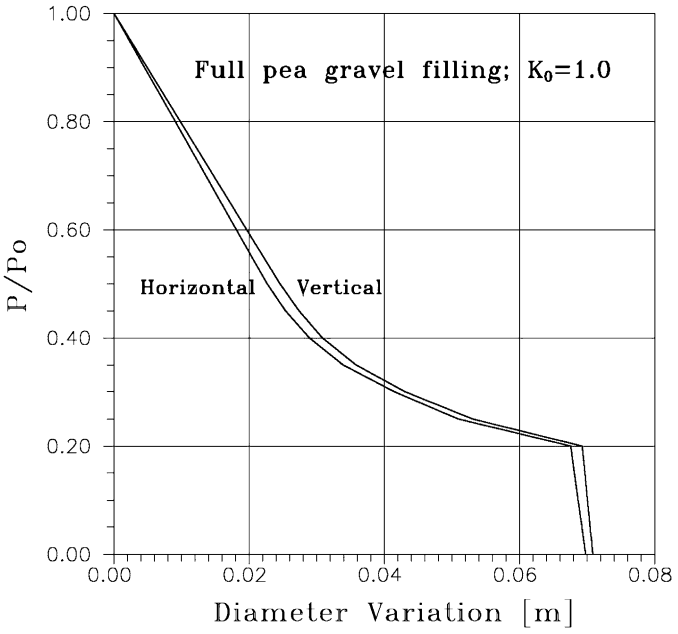

Fig. 12. Convergence-confinement curve for $K_0 = 1.0$

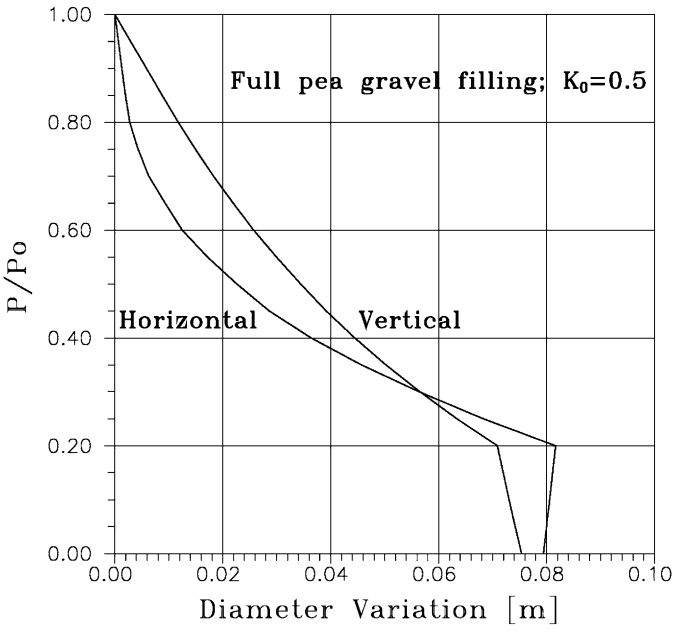

Fig. 13. Convergence-confinement curve for $K_0 = 0.5$

Int. J. Geomech. 2012.12:722-731.

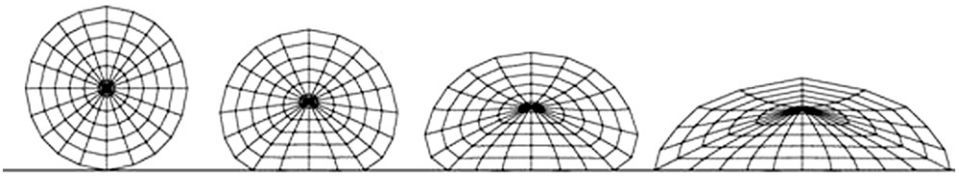

Fig. 14. Deformation of a viscoplastic disc subjected to its self-weight and resting on a rough rigid plane

each analysis. The stiffness matrix was reassembled considering the updated coordinates when the increment of displacements reached a given small tolerance.

Note that the FE mesh used for calibrating the material parameters of the strain softening concrete (see Fig. 8) adopted elements smaller than those used in the tunnel analyses (see Fig. 11). To reduce the mesh dependency of the results, the parameters where scaled with respect to those derived from the laboratory tests according to the findings of Pietruszczak and Stolle (1985). A series of initial steps in which the liner and the PG were not active brought P to 20% of geostatic pressure P_0. Then, the lining elements and those representing the lean concrete zone (see Fig. 2) were activated. Also, the PG interface was activated except for the portion close to the tunnel crown defined by angle α in Fig. 11.

The analysis continued with further decrements of P tracking the position of the nodes belonging to the external surface of the liner. When one of these nodes (for example, Node A) intersected a side (for example, Side B) of an element discretizing the opening contour, a so-called multipoint constraint (MPC) was introduced, constraining Node A to move alongside B, and the stiffness matrix was modified accordingly. The nodal forces at Node A in the directions tangent and normal to Side B were evaluated and, through the elastic-plastic algorithm based on the modified Newton-Raphson method (Zienkiewicz et al. 1969), the shear component was kept within the limit governed by the shear resistance of the rock-liner interface. The MPC was eliminated if a tensile normal component was calculated. Considering the limited displacements expected in the present context, this approximated procedure should not lead to grossly incorrect results. An illustrative example is shown in Fig. 14.

Various analyses were performed on the tunnel by varying extension α of the empty gap. For sake of briefness, only the results of two analyses are illustrated here for $\alpha = 67$ and 45°, which correspond to empty gaps of 134 and 90° above the crown. Fig. 15 shows the diagrams relating the variations of the vertical and horizontal diameters of the lining to the pressure P for $\alpha = 67°$. The liner and partial filling of PG were set in place when the pressure reached 20% of the in situ stresses. Fig. 16 shows the contour lines of the square root of the second invariant of the deviatoric plastic strains within the liner corresponding to various stages of the analysis, referred to as I–IV in Fig. 15.

Initially, the deformation of the liner developed almost linearly until the condition represented by Point I in Fig. 15 was reached. The horizontal diameter decreased, while the vertical diameter increased because of the lack of contact between the liner and rock at the crown. In Condition I no plastic strains were present in the liner [see Fig. 16(a)]. Then, the displacements increased rapidly from I to II as a result of the onset of fractures at the tunnel crown and springlines [see Fig. 16(b)]; however, no contact was established between the liner and rock at the crown.

A further decrease of P created Condition III where the closure of the rock-liner gap at the crown occurred [see Fig. 16(c)]. Subsequently, the increase of the vertical and horizontal pressures on

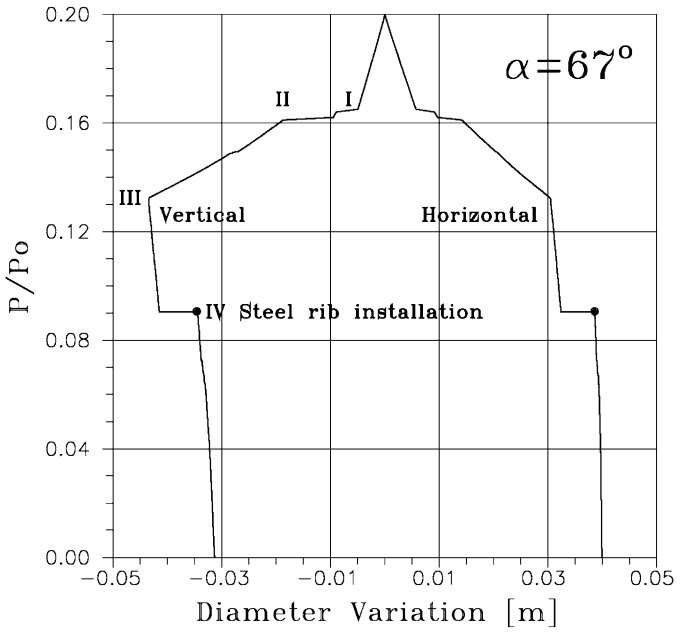

Fig. 15. Variations of the horizontal and vertical diameters of the liner with decreasing pressure P for $\alpha = 67°$

the liner produced a reduction of both the vertical and horizontal diameters until Condition IV was reached [see Fig. 16(d)]. A lack of convergence of the elastic-plastic algorithm occurred at this stage, which corresponded to the lining failure caused by the excessive spreading of the fractured zones. To avoid collapse, beam elements equivalent to the supporting steel ribs were introduced at IV. This provision ensured the stability of the opening and permitted completing the numerical analysis without further spreading of cracks.

Even though the described results provide some insight into the evolution of damage in the liner, they present a substantial drawback by not reproducing the actual distribution of the fractures observed in the tunnel. In fact, while three fractured zones were observed at most sections—one at the crown and two at the springlines—the numerical analysis predicted the formation of five damaged zones.

The calculations were them repeated by decreasing the extension of the empty gap to $\alpha = 45°$. These results are summarized in Figs. 17 and 18, which show the same kind of diagrams previously given for $\alpha = 67°$. In this case, the final distribution of damage [see Fig. 18(c)] was quite similar to that actually observed in the field. Also for $\alpha = 45°$, the introduction of steel ribs was necessary to avoid collapse. Two alternatives were considered, which consisted of two HE 140 B or two HE 140 M ribs for each liner ring. The corresponding distributions of the maximum axial stress within the ribs at the end of analyses are shown in Fig. 19, where s denotes the curvilinear abscissa from the tunnel crown and S_0 is the total length of the liner contour. If steel FE 510 with a limit stress of 355 MPa is

Int. J. Geomech. 2012.12:722-731.

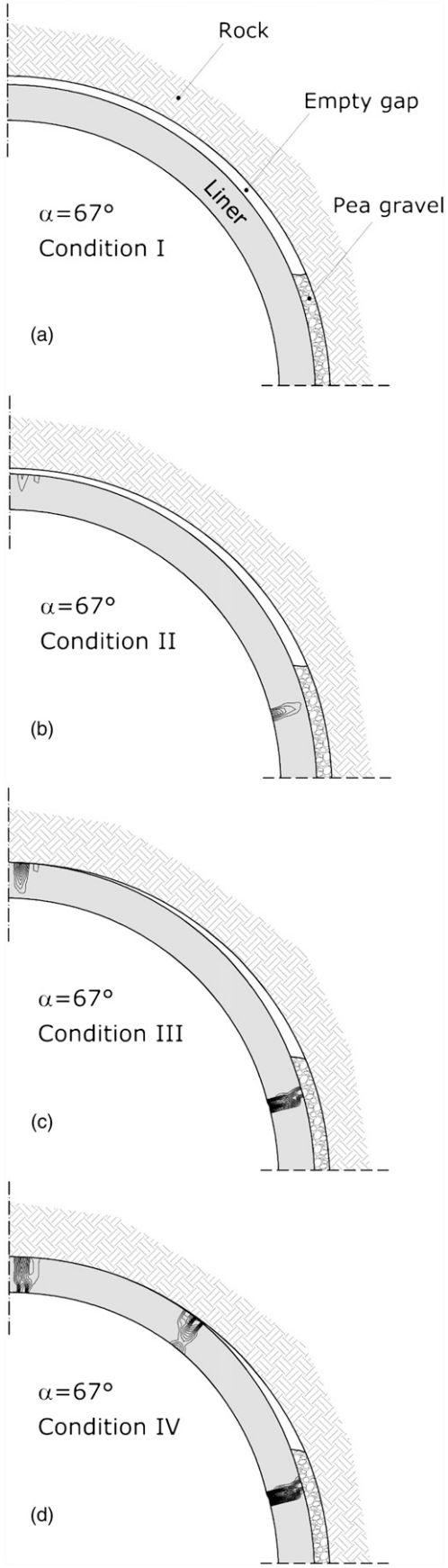

Fig. 16. Spreading of the deviatoric plastic strains within the liner for $\alpha = 67°$

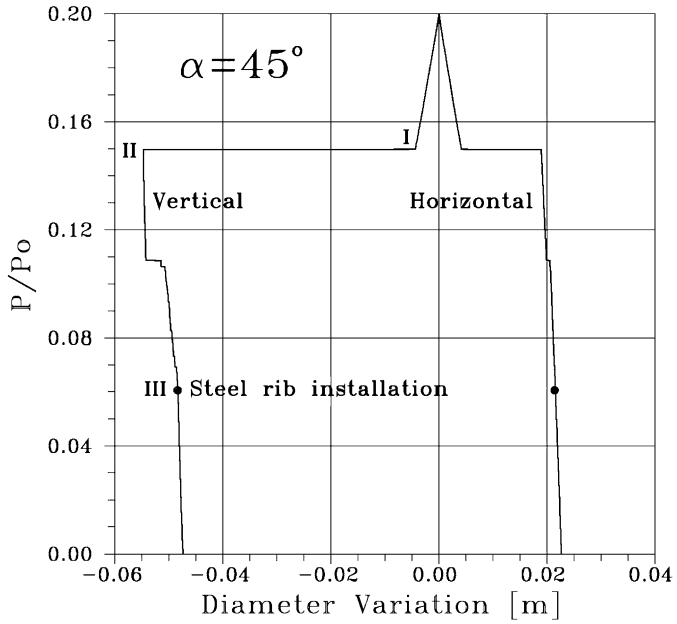

Fig. 17. Variation of the horizontal and vertical diameters of the liner with decreasing pressure P for $\alpha = 45°$

used for the ribs, considering that the upper value of the compressive normal stress slightly exceeds 150 MPa, this provision seems adequate for stabilizing the opening with an acceptable factor of safety.

Alternative Stabilization Procedures

It was previously observed that the steel ribs permit a rapid and effective stabilization of the opening. However, their use presents the notable drawback of not preventing the formation of cracks in additional rings over time. Furthermore, they involve a reduction of the available section of the tunnel. Consequently, the choice of a different method for structural rehabilitation seemed advisable (Locatelli et al. 2004, 2005).

Perhaps the most effective method would be the demolition of the present rings and the construction of a new cast-in-place, reinforced-concrete lining. However, besides its cost such a choice would require the removal of the pipeline contained within the tunnel for the duration of the works, and this is not possible for a series of important social and economic reasons. Also, the installation of anchors or bolts does not seem possible because the fractured state of many rings would limit their effectiveness.

The remaining alternative consists in the injection of grouting to fill the voids between the liner and rock to reestablish a continuous pressure distribution on the liner. If this condition were achieved, the concrete segments would support the estimated rock load with an adequate margin of safety. In fact, the calculations for the fully grouted gap indicated a maximum compressive stress in the lining of the order of 30 MPa, while the compressive strength of the fiber-reinforced concrete ranged between 73 and 119 MPa.

Considering that further injections of PG do not seem advisable because they would not guarantee a complete filling of all voids, it was suggested to adopt a grouting mixture of cement mortar. This, in addition, would consolidate the PG layer, providing an appreciable cohesion to it and increasing the overall bearing capacity of the annular support. Considering that it is not possible to identify all sections prone to future damage, it was suggested to extend the treatment to the entire tunnel.

Int. J. Geomech. 2012.12:722-731.

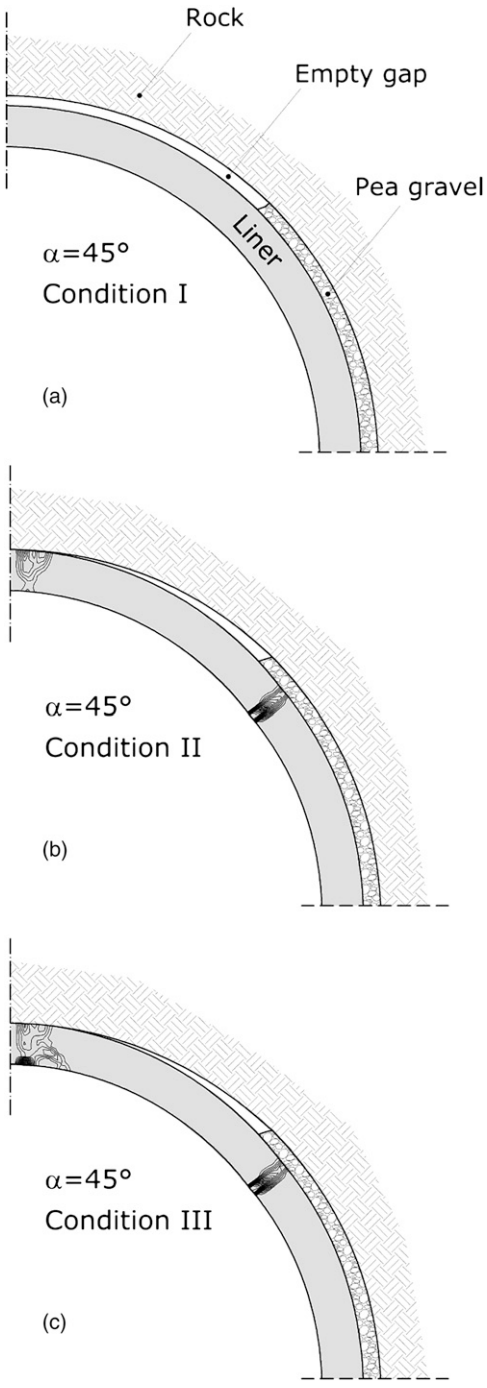

Fig. 18. Spreading of the deviatoric plastic strains within the liner for $\alpha = 45°$

The injections were carried out in subsequent portions of the tunnel after sealing the cracks and the open waterstop joints to prevent the leakage of mortar within the tunnel. The treatment proceeded from the bottom to the top of the ring through a series of radial holes. A valve placed in each hole prevented leakage of the mortar at the end of the grouting phase. The pressure injection ranged between 0.5 and 0.8 MPa and the volume of grouting was controlled to estimate the complete filling of the voids.

At the end of the treatment some borings were made through the liner and a ground-penetrating radar survey was carried out for each treated part of the tunnel to check the presence of still empty zones

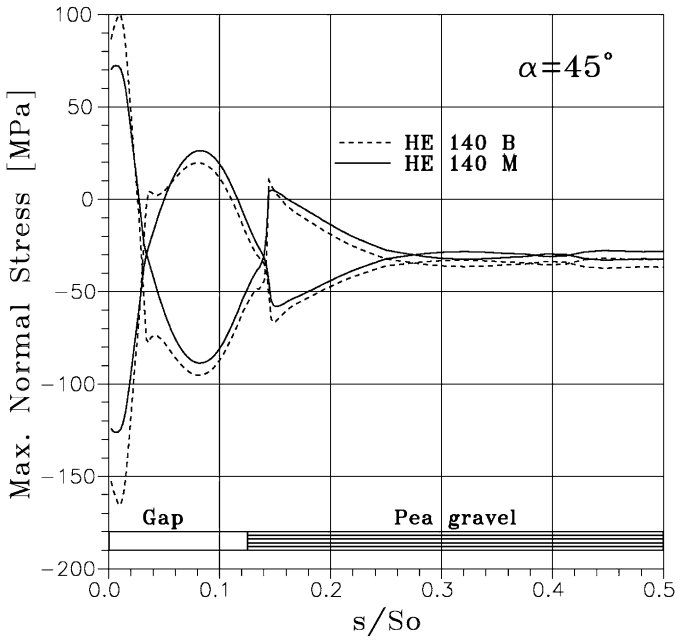

Fig. 19. Variation with curvilinear abscissa s from the tunnel crown of the maximum normal stress in the steel ribs for $\alpha = 45°$

within the gap. The described provision turned out to be effective; in fact, no further progress of damage was observed in the previously treated sections. After completing the backfill, the steel ribs will be removed in a few tunnel sections, controlling the deformation of the corresponding rings. If no local damage is produced, the removal will be extended to the entire tunnel.

Concluding Remarks

The causes that led to severe damage of the segmented precasted concrete liner of a deep tunnel have been illustrated. Experimental and numerical investigations were carried out, which suggest the following. The main cause of damage is likely to be the incomplete PG filling of the gap existing between the liner and the surrounding rock. The liner presented an overall brittle behavior and, as a consequence, was particularly prone to fracturing. This depended on the fact that standard steel bars were absent in the concrete segments, which were reinforced solely by steel fibers. It seems reasonable to conclude that the damage would have been less severe if steel bars and stirrups were used instead. Also, the use of PG contributed to the spreading of damage. This depends on the inherent difficulties in ensuring a uniform filling of the annular void with injections of granular material. Perhaps a better result could have been obtained by using concrete mortar as the grouting material during the tunnel construction.

The empirical criterion developed for the rational choice of the sections where steel ribs have to be installed, as the damage spreads over time, turned out to be effective and prevented the possible collapse of the fractured rings. The numerical analyses provided some insight into the rock-liner interaction and led to a proper dimensioning of the steel ribs. This provision is rapid and effective; however, it presents the drawback of reducing the available internal section of the tunnel. To overcome this problem, an alternative method was subsequently applied based on injections of cement mortar within the rock-liner gap throughout the entire tunnel. This method was apparently successful because no further damage was observed at the restored

Int. J. Geomech. 2012.12:722-731.

sections. The removal of the steel ribs could be then undertaken, carefully controlling the stability of the restored portions of the liner.

References

Association Française des Tunnels et de l'Espace Souterrain (AFTES). (1993). "Considerations on the usual methods of tunnel lining design." *GT7R2A1*, AFTES, Paris, 165−187.

Cividini, A., and Gioda, G. (1992). "Finite element analysis of direct shear tests on stiff clays." *Int. J. Numer. Analyt. Meth. Geomech.*, 16(12), 869−886.

Contini, A., Cividini, A., and Gioda, G. (2007). "Numerical evaluation of the surface displacements due to soil grouting and to tunnel excavation." *Int. J. Geomech.*, 7(3), 217−226.

Falliti, P., and Marchiori, S. (2003). "Galleria Sorenberg: Scavo con TBM in ambiente esplosivo." *Guida al tunneling*, M. Bringiotti, ed., Pei, Parma, Italy, 187−192.

Locatelli, L., Borgonovo, G., and Gioda, G. (2004). "A consistent approach to the structural rehabilitation of tunnel liners." *Proc., 18th TAC National Conf. on Advances in Tunnelling and Trenchless Techniques*, C. D. Martin, ed., Edmonton, Canada, Tunnelling Association of Canada, 25, 1−10.

Locatelli, L., Borgonovo, G., and Gioda, G. (2005). "A design procedure for the rehabilitation of tunnel liners." *Proc., 11th Conf. of the International Association for Computer Methods and Advances in Geomechanics*, G. Barla and M. Barla, eds., Patron, Bologna, Italy, Vol. 3, 35−42.

Pietruszczak, S., and Stolle, D. F. E. (1985). "Deformation of strain softening materials. Part I: objectivity of finite element solution based on conventional strain softening formulation." *Comput. Geotech.*, 1(2), 99−115.

Sterpi, D., and Gioda, G. (2009). "Visco-plastic behaviour around advancing tunnels in squeezing rock." *Rock Mech. Rock Eng.*, 42(2), 319−339.

Zienkiewicz, O. C., Valliappan, S., and King, I. P. (1969). "Elasto-plastic solutions of engineering problems 'initial stress,' finite element approach." *Int. J. Numer. Methods Eng.*, 1(1), 75−100.